Available online at www.sciencedirect.com
ScienceDirect
Journal of the European Ceramic Society 27 (2007) 2629–2634
www.elsevier.com/locate/jeurceramsoc

Synthesis of ultra thin α-alumina nanobelts from aluminum powder by chemical vapor deposition

C.Y. To, L.Y. Cheung, Y.F. Li, K.C. Chung, Daniel H.C. Ong, Dickon H.L. Ng *

Department of Physics, The Chinese University of Hong Kong, Shatin, Hong Kong, China

Received 29 July 2006; received in revised form 15 November 2006; accepted 25 November 2006
Available online 24 January 2007

Abstract

Ultra thin α-alumina nanobelts with single-crystalline rhombohedral structure were obtained by oxidizing Al in moisturized air under reduced pressure. It was found that the length and width of the nanobelts increased with sintering time. By preparing the samples in different environments, it was demonstrated that the presence of oxygen was essential to the formation of the alumina nanobelts, while the presence of water vapor substantially increased the yield. The epitaxial growth of the nanobelts was also studied. Belts tended to grow parallel to the (0 0 0 1) sapphire substrate, but 60° and 90° to the (1 0 $\bar{1}$ 0) and the (1 1 $\bar{2}$ 0) substrates, respectively. The vapor–solid mechanism and molecule impinging model were proposed to describe the growing process. This method provides a simple and cost-effective route for preparing α-alumina nanobelts.

Keywords: Al_2O_3; Sintering; Microstructure-final

1. Introduction

One-dimensional nanowires and nanobelts have attracted extensive interests due to their wide range of potential applications. Various kinds of binary oxide nanobelt and nanowire products, such as Ga_2O_3,[1] ZnO[2], and Al_2O_3[3,4] have been reported in recent years. Since there are great demands for nanometer-sized materials with extraordinary optical, electrical, magnetic, and mechanical properties, exploration of methods for the large-scale productions of these types of materials remains a challenging task. Ceramic alumina (Al_2O_3) is an important structural material owing to its high melting point and resistance to deformation. Efforts have been put forward to obtain nanostructured alumina. Currently, nano-alumina have been obtained by catalyst-supported chemical vapor deposition (CVD),[5–7] or by the in situ displacement reactions.[8–10] In many of these fabrication methods, it is usually not possible to obtain pure products without having impurities. While catalyst-free CVD process like carbothermal synthesis[4] which uses graphite and oxygen, or uses water vapor as oxidizing agent,[3] can produce pure alumina products, a thermal gradient is often needed. In these CVD processes, products are to be deposited in a lower temperature zone, and higher temperature (>1300 °C) is required to vaporize the Al source at the other end. In this article, we report the fabrication of ultra thin α-alumina nanobelts through a simple catalyst-free CVD method. Inexpensive starting materials, namely Al powder and water vapor are utilized. At the same time, establishment of a thermal gradient zone is not required and only a relatively low temperature (1150 °C) is needed. These simplify the experimental setup and reduce the production cost.

2. Experimental procedures

Pure Al powder (99.7% purity, −325 mesh, STREM Chemicals Inc., Newburyport, MA) was placed in an alumina boat. A polycrystalline alumina wafer was placed 6 mm above the boat. The entire setup was inserted horizontally into a tube furnace. The system was connected to a rotary pump, and a pressure of 4 Torr was maintained. Water moisture was introduced by bubbling air through distilled water at room temperature in a sealed flask before it was released into the system. The temperature in the furnace was raised to 1150 °C at a rate of 20 °C/min. A series of samples were collected after they were separately held at this target temperature for different durations ranging from 15 min to 4 h. For comparison, two other samples were sintered in moisturized Ar and in dry air for 1 h. In preparing the

* Corresponding author. Tel.: +85 22 609 6392; fax: +85 22 603 5204.
E-mail address: dng@phy.cuhk.edu.hk (D.H.L. Ng).

0955-2219/$ – see front matter © 2006 Elsevier Ltd. All rights reserved.
doi:10.1016/j.jeurceramsoc.2006.11.077

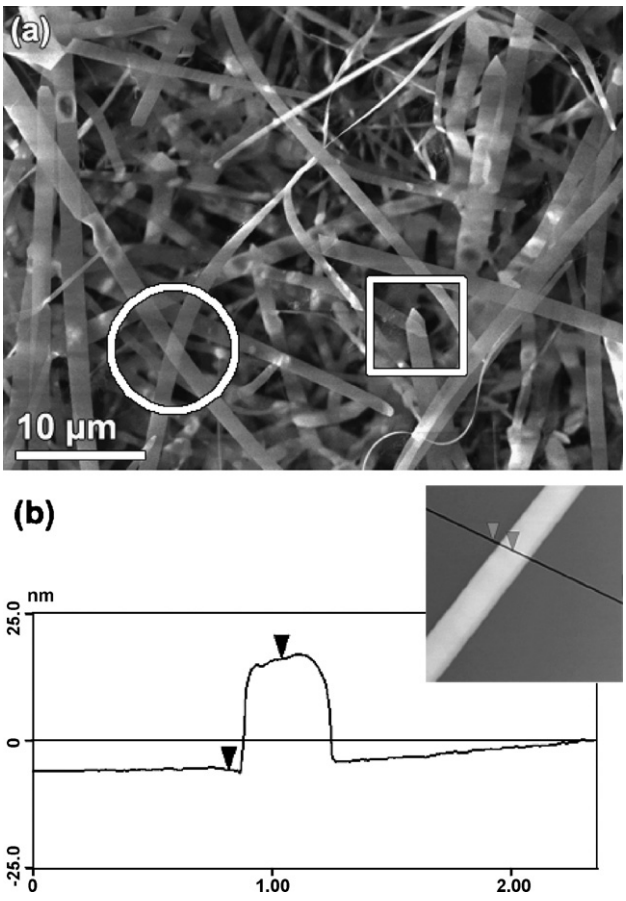

Fig. 1. (a) SEM micrograph of alumina nanobelts grown on a polycrystalline alumina substrate. (b) Thickness of a nanobelt was estimated by using AFM.

moisturized Ar, high purity Ar (99.995%) was bubbled through distilled water before it was allowed to enter the system. To study the epitaxial growth of the alumina products on the substrate, sapphire wafers (from Shanghai Shentai New Inorganic Materials Co. Ltd., China) with orientations of (0 0 0 1), (1 0 $\bar{1}$ 0), and (1 1 $\bar{2}$ 0) were employed for deposition under the same condition. The morphology and composition of the as-prepared products on the sapphire substrates were characterized. Microstructural characterization was performed by scanning electron microscopy (SEM, LEO 1450VP, Thronwood, NY) and transmission electron microscopy (TEM, CM120, Philips, Hillsboro, OR). Elemental and chemical analyses were carried out by energy dispersive X-ray spectrometry (EDS). Higher magnification morphological characterization was performed by using atomic force microscopy (AFM, Nanoscope III, Veeco Digital Instrument, Woodbury, NY) and high-resolution transmission electron microscopy (HRTEM, Tecnai 20, Hillsboro, OR).

3. Results and discussion

3.1. General results

A layer of white film was found on the polycrystalline alumina substrate after the system was held at 1150 °C in the presence of moisturized air for an hour. Fig. 1(a) is a SEM micrograph taken from the surface of the substrate. A large number of nanobelts were found. Each belt was with straight side edges and uniform width along its longitudinal axis. The average width and length was ∼1.5 and over ∼100 μm, respectively. We also observed that the belts were rather thin. As seen from the cir-

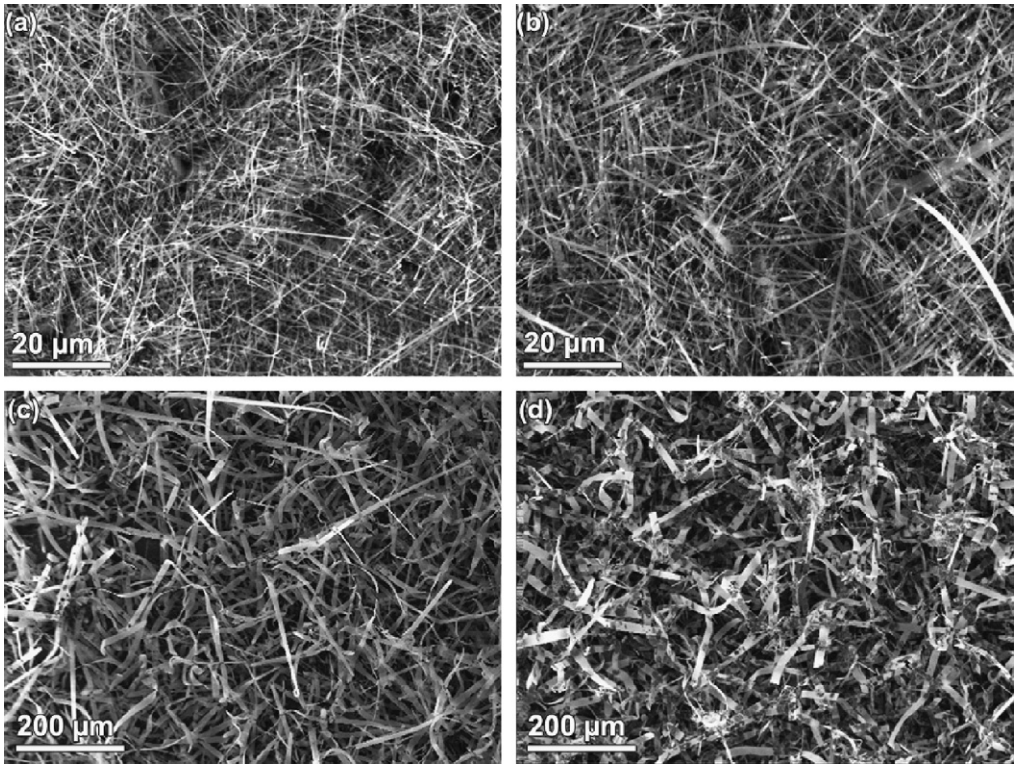

Fig. 2. SEM images of the nanobelts on samples sintered in moisturized air for (a) 0.25 h, (b) 0.5 h, (c) 2 h, and (d) 4 h.

cled region in the image (Fig. 1(a)), even an electron beam with a rather low accelerating voltage (~10 kV) was able to penetrate through them. By using AFM, we determined that the thickness of a selected nanobelt was ~21 nm, and the result is shown in Fig. 1(b).

3.2. Effects of sintering time

To study the growth of nanobelts at different stages, four more samples were prepared for comparative studies. They were sintered separately at 1150 °C for 0.25, 0.5, 2 and 4 h in moisturized air. The results are shown in Fig. 2(a–d), respectively. We found that belt-like structures were obtained from these samples, while the length and width of the belts increased with holding time. The average width of the belts increased from ~360 nm in the sample sintered for 0.25 h, to ~15 μm in the sample sintered for 4 h, and the corresponding length increased from ~40 to over ~200 μm.

Some of the belts from the 4-h sample were extracted, and were examined by using TEM and HRTEM. The TEM image in Fig. 3(a) shows the tip of one of these belts. The tip was triangular, at which only Al and O were detected by EDS (bottom right inset in Fig. 3(a)). The single crystalline nature at the tip was confirmed by the clear diffraction pattern, shown in the bottom left inset in Fig. 3(a), which was obtained by selected area electron diffraction (SAED). This pattern was associated with the [0 0 0 1] zone axis, and was indexed to be a rhombohedral structure with $R\bar{3}c$(167) symmetry (based on JCPDS Card No: 46-1212). Applying the out-of-focus technique to the diffraction spots, we determined that the growth direction of the belt was in the [1 1 $\bar{2}$ 0] direction. This result was consistent with another report[11] which studied the growth direction of alumina whiskers. Fig. 3(b) shows an HRTEM image of a magnified region near the edge of the nanobelt. The lattice spacings parallel and normal to the growth direction of the belt were determined to be 0.237 and 0.138 nm, which corresponded to the (1 1 $\bar{2}$ 0) and (1 0 $\bar{1}$ 0) planes of alumina, respectively. The micrograph also indicated that this belt was free from dislocations, and its tip was perfectly crystalline.

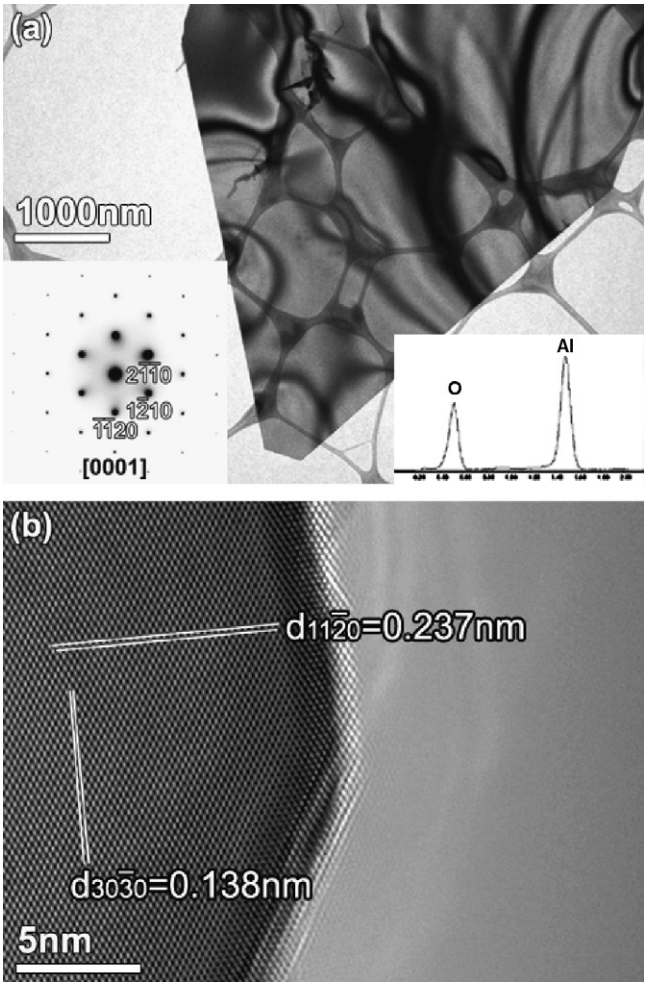

Fig. 3. (a) TEM image shows the tip of a nanobelt. The bottom left inset shows its corresponding SAED pattern. The bottom right inset shows its EDS spectrum. (b) HRTEM image of the edge of the nanobelt.

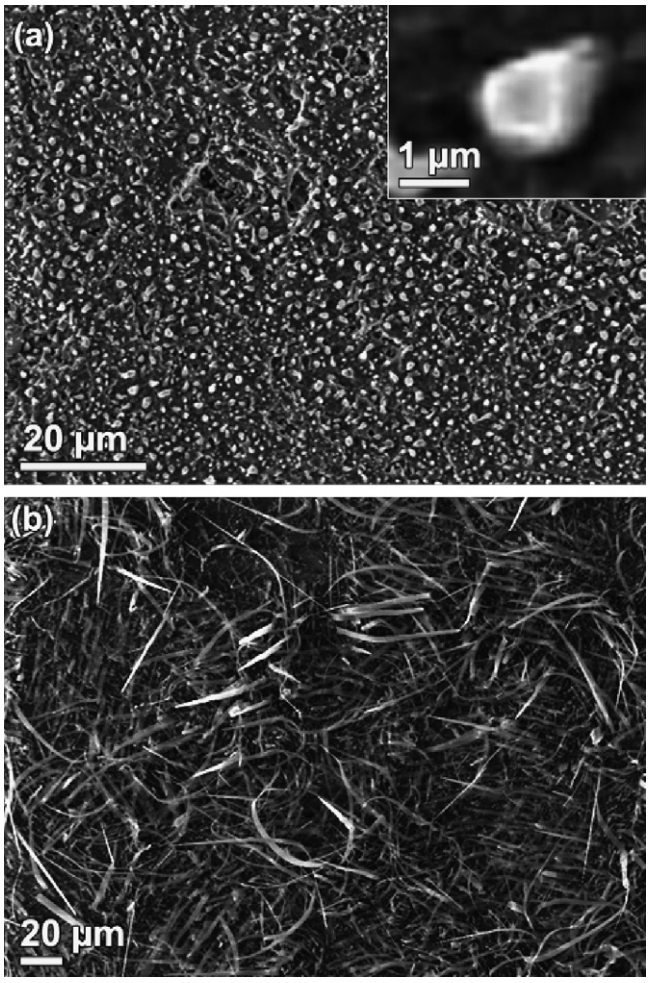

Fig. 4. SEM images of the samples prepared in (a) moisturized argon and (b) dry air.

3.3. Effects of sintering environment

To verify that air was essential to the formation of these alumina nanobelts, a sample was sintered in moisturized argon for 1 h. Fig. 4(a) shows a SEM image of this sample. No belt-like

feature was found, and only particles of about 1 μm in diameter were observed. The EDS analysis revealed that these particles contained Al and O, suggesting that they were alumina particles. The SEM image in Fig. 4(b) shows another sample which had been sintered in dry air for 1 h. Similar to those samples sintered in moisturized air, belt-like structures were obtained, and the EDS analysis revealed that they contained Al and O. Results from the same characterization procedures showed that the crystalline structure and growth direction of these nanobelts were identical to those prepared in moisturized air. However, the yield of the nanobelts prepared in dry air was significantly less. Furthermore, the average length and width of these belts were only 40 and 4 μm, respectively. Their aspect ratio was about 10, which was ten times smaller than that of the nanobelts in the sample prepared in moisturized air.

3.4. Epitaxial growth

In the study of the epitaxial growth of these belts, samples were grown separately on three different sapphire substrates with orientations of (0 0 0 1), (1 0 $\bar{1}$ 0) and (1 1 $\bar{2}$ 0) under the same condition, i.e., at 1150 °C for 1 h in moisturized air. The nanobelts grown on the (0 0 0 1) substrate are shown in Fig. 5(a), in which they appeared short. As indicated by the arrows, the as-grown belts showed a three-fold symmetry on their preferential growth. A schematic diagram is shown in Fig. 6(a) to illustrate the development of such a symmetry. Since the [1 1 $\bar{2}$ 0] direction lay on the (0 0 0 1) plane, it was not possible for the belts having the preferred ⟨1 1 $\bar{2}$ 0⟩ to grow perpendicularly away from the (0 0 0 1) plane of sapphire, thus precursors were needed. As a consequence, nucleation and growth of precursors on the (0 0 0 1) plane must take place before the belts were allowed to grow on the {1 1 $\bar{2}$ 0} planes of the precursors. Fig. 5(b) shows the sample prepared on the (1 0 $\bar{1}$ 0) substrate. The image is a side view of the sample with the growth directions of the belts indicated by the arrows. The angle between these arrows was about 60°, and the value matched well with the angle between two {1 1 $\bar{2}$ 0} planes. When the sample was viewed from the top (inset of Fig. 5(b)), no preferred orientation was observed. Fig. 5(c) and its inset show the side view and top view of the belts grown on the (1 1 $\bar{2}$ 0) substrate. As indicated by the arrow, the growth direction of the belts was normal to the substrate. The above observations revealed that the orientation of the substrate had a direct impact on the growth of these belts.

3.5. Mechanism of formation

In this work, no intended catalyst was used in the experiments, and no foreign droplet was observed at the tips of the nanobelts (Figs. 1 and 3(a)). We propose that the growth of these alumina nanobelts followed the vapor–solid (VS) mechanism. In the initial stage, as temperature was increased beyond the melting point of Al, the Al powder melted and vaporized to form Al vapor under a reduced pressure at 4 Torr, thus,

$$Al_{(s)} \rightarrow Al_{(l)} \rightarrow Al_{(g)} \quad (1)$$

where s, l, and g indicated whether the reactant or product was in the form of solid, liquid, or gas, respectively. In the stage that followed, there were several possible paths for the Al vapor to be converted to Al_2O_3. Based on the data given in the thermochemical tables,[13] Hargraves[12] had laid out the formulations of the Gibbs energies of formation (ΔG) for the possible reactions between Al and H_2O or O_2. The reactions and their corresponding ΔG values at 1150 °C are given below:

$$2Al_{(g)} + H_2O_{(g)} \rightarrow Al_2O_{(g)} + H_{2(g)} \quad (\Delta G = -92\,\text{kJ/mol}) \quad (2)$$

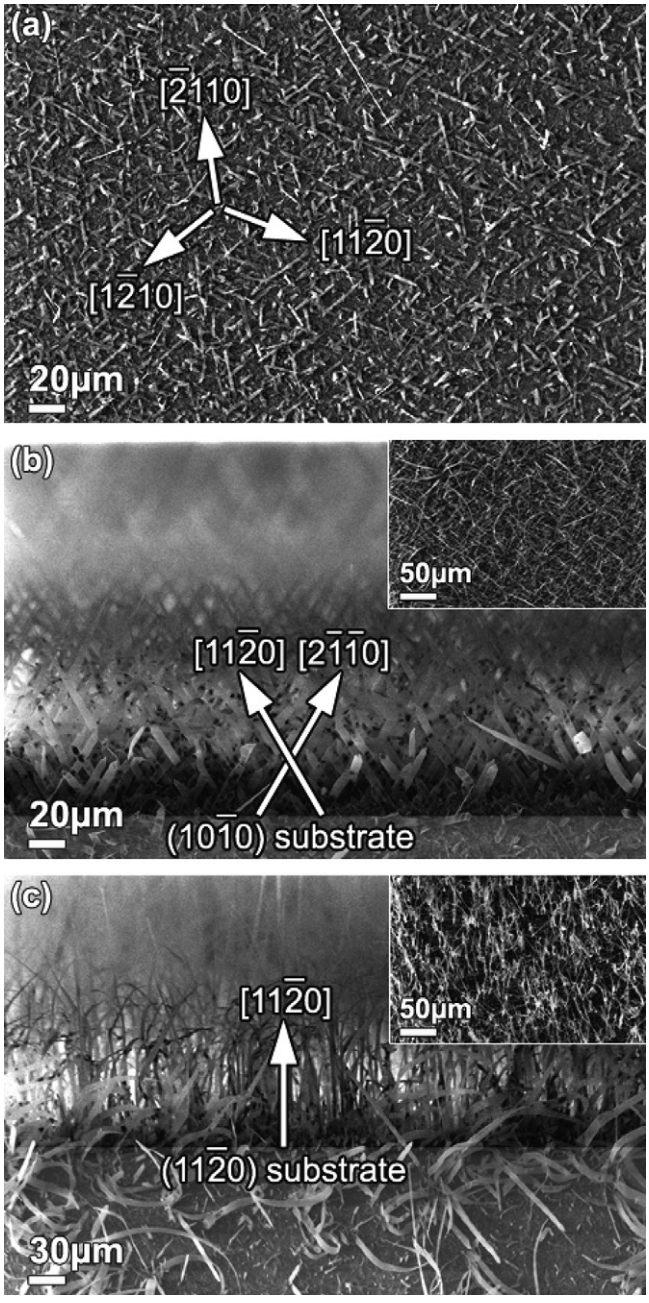

Fig. 5. SEM images of sintered samples. (a) Top view of the (0 0 0 1) sapphire substrate, (b) side view of the (1 0 $\bar{1}$ 0) substrate (inset shows the top view), and (c) side view of the (1 1 $\bar{2}$ 0) substrate (inset shows the top view).

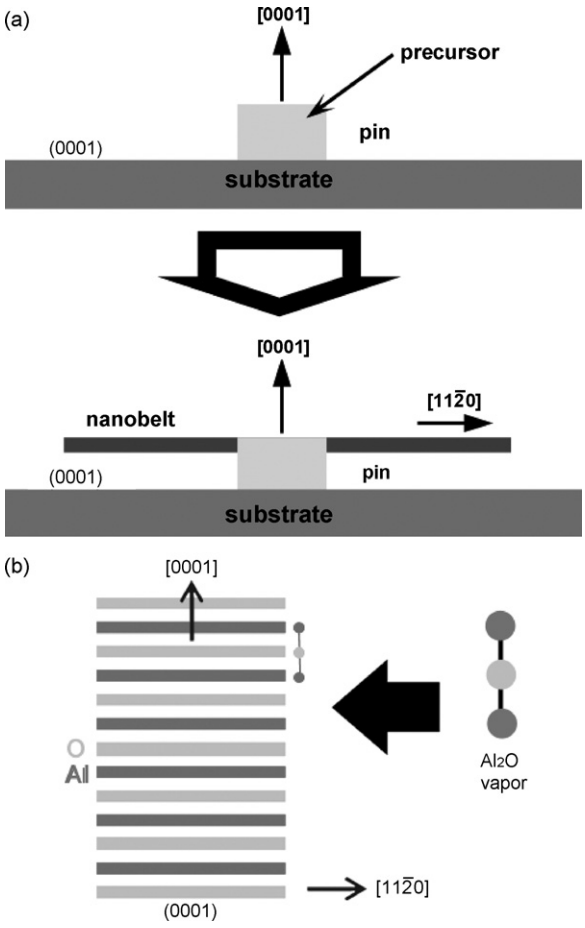

Fig. 6. Schematic diagrams show: (a) the growth of nanobelts on the (0 0 0 1) sapphire substrate and (b) an Al_2O molecule attaching onto the (1 1 $\bar{2}$ 0) plane.

$$4Al_{(g)} + O_{2(g)} \rightarrow 2Al_2O_{(g)} \quad (\Delta G = -502\,kJ/mol) \tag{3}$$

$$2H_{2(g)} + O_{2(g)} \rightarrow 2H_2O_{(g)} \quad (\Delta G = -338\,kJ/mol) \tag{4}$$

$$Al_2O_{(g)} + O_{2(g)} \rightarrow Al_2O_{3(s)} \quad (\Delta G = -979\,kJ/mol) \tag{5}$$

Initially, Al vapor reacted with water vapor or oxygen gas to form Al_2O gas as stated in reactions (2) or (3). The resultant hydrogen gas reacted with oxygen gas to produce water vapor via reaction (4), and more Al_2O gas was then produced from water vapor by reaction (2). The Al_2O gas further oxidized to form Al_2O_3 through reaction (5). This freshly formed Al_2O_3 acted as the precursors. In the steady state, the Al_2O molecules tended to attach onto the {1 1 $\bar{2}$ 0} surfaces of these alumina precursors and led to the growth of the nanobelts.

The Al_2O molecules were the dominant intermediate products of the initial reactions. They exhibit a linear structure.[14] During the growth of these nanobelts, Al_2O did not favor the growth of the belts on the (0 0 0 1) plane of the Al_2O_3 precursor. It was because such a plane could not accommodate the Al_2O molecule having a linear structure,[14] whereas the situation was entirely different for the (1 1 $\bar{2}$ 0) plane. A schematic diagram is shown in Fig. 6(b) to illustrate the so-called Al_2O molecule impinging model.[15,16] The Al_2O molecules preferably attached onto the (1 1 $\bar{2}$ 0) plane of the precursor, which was oriented perpendicularly to the [0 0 0 1] direction. The remaining O sites on the (1 1 $\bar{2}$ 0) plane were filled by the oxygen atoms supplied from reaction (5), thus the surface charge stoichiometry of the (1 1 $\bar{2}$ 0) plane was maintained. Subsequently, the nanobelts would preferably be grown epitaxially along the [1 1 $\bar{2}$ 0] direction.

4. Conclusions

The ultra thin α-alumina nanobelts were synthesized through a simple CVD method at a relatively low temperature in reduced pressure. The morphology and composition were characterized, and the growth mechanism was studied. We found that increasing the sintering time increased the length and width of the nanobelts. Moisturized air was essential in preparing Al_2O_3 nanobelts, and the presence of water vapor promoted its yield. The VS model was proposed to explain the growth of the nanobelts. The epitaxial growth was studied and the mechanism was explained by the Al_2O molecule impinging model.

Acknowledgement

This work was supported by the RGC Earmarked Research Grant (2004/05) from the Hong Kong SAR Government (CUHK Project code: 2150421; Reference No. 4233/04E).

References

1. Xiang, X., Cao, C. B., Guo, Y. J. and Zhu, H. S., A simple method to synthesize gallium oxide nanosheets and nanobelts. *Chem. Phys. Lett.*, 2003, **378**, 660–664.
2. Yi, G. C., Wang, C. and Park, W. I., ZnO nanorods: synthesis, characterization and applications. *Semicond. Sci. Technol.*, 2005, **20**, S22–S34.
3. Fang, X. S., Ye, C. H., Peng, X. S., Wang, Y. H., Wu, Y. C. and Zhang, L. D., Temperature-controlled growth of α-Al_2O_3 nanobelts and nanosheets. *J. Mater. Chem.*, 2003, **13**, 3040–3043.
4. Rao, C. N. R., Gundiah, G. F., Deepak, F. L., Govindaraj, A. and Cheetham, A. K., Carbon-assisted synthesis of inorganic nanowires. *J. Mater. Chem.*, 2004, **14**, 440–450.
5. Valcárcel, V., Cerecedo, C. and Guitián, F., Method for production of α-alumina whisker via vapor–liquid–solid deposition. *J. Am. Ceram. Soc.*, 2003, **86**(10), 1683–1690.
6. Zhu, Y. Q., Jin, Y. Z., Kroto, H. W. and Walton, D. R. M., Co-catalysised VLS growth of novel ceramic nanostructures. *J. Mater. Chem.*, 2004, **14**, 685–689.
7. Schreiner, M., Wruss, W. and Lux, B., Growth Morphology and growth mechanism of α-Al_2O_3 whiskers. *J. Cryst. Growth*, 1983, **61**, 75–79.
8. Deng, C. J., Yu, P., Yau, M. Y., Ku, C. S. and Ng, D. H. L., Fabrication of single-crystal α-Al_2O_3 nanorods by displacement reactions. *J. Am. Ceram. Soc.*, 2003, **86**, 1385–1388.
9. Tang, C. C., Fan, S. S., Li, P., Chapelle, M. L. and Dang, H. Y., In situ catalytic growth of Al_2O_3 and Si nanowires. *J. Cryst. Growth*, 2001, **224**, 117–121.
10. Fang, X. S., Ye, C. H., Xu, X. X., Xie, T., Wu, Y. C. and Zhang, L. D., Synthesis and photoluminescence of α-Al_2O_3 nanowires. *J. Phys.: Condens. Matter*, 2004, **16**, 4157–4163.
11. Minagawa, S., Kinetics of growth of Al_2O_3 whiskers. *J. Am. Ceram. Soc.*, 1972, **55**, 77.
12. Hargraves, C. M., On the growth of sapphire microcrystals. *J. Appl. Phys.*, 1961, **28**, 936–938.

13. Malcolm, W. and Chase, J. R., *NIST-JANAF Thermochemical Tables* (*4th ed.*). American Chemical Society, Woodbury, New York, 1998.
14. Koput, J. and Gertych, A., Ab initio prediction of potential energy surface and vibrational-rotational energy levels of di-aluminum monoxide, Al_2O. *J. Chem. Phys.*, 2004, **121**, 130–135.
15. Wang, Z. L., Functional oxide nanobelts: properties and potential applications in nanosystems and biotechnology. *Annu. Rev. Phys. Chem.*, 2004, **55**, 159–196.
16. Dai, Z. R., Pan, Z. W. and Wang, Z. L., Novel nanostructures of functional oxides synthesized by thermal evaporation. *Adv. Funct. Mater.*, 2003, **13**, 9–24.